Crimson Publishers
Wings to the Research

Review Article

Preparation, Physical and Photo-Electrochemical Characterization of the Bojarite Mineral $Cu_3(trz)_3(\mu_3\text{-}OH)]Cl_2.6H_2O$ at Low Temperature

Bagtache R*, Douba W, Lahmek A, Djaballah AM and Trari M

Faculty of Chemistry, University of Science and Technology Houari Boumediene, Algeria

ISSN: 2770-6745

***Corresponding author:** Bagtache R, Laboratory of Electrochemistry-Corrosion, Metallurgy and Inorganic Chemistry, Faculty of Chemistry, (USTHB), BP 32, 16111, Algiers, Algeria

Submission: July 11, 2025
Published: September 15, 2025

Volume 5 - Issue 4

How to cite this article: Bagtache R*, Douba W, Lahmek A, Djaballah AM and Trari M. Preparation, Physical and Photo-Electrochemical Characterization of the Bojarite Mineral $Cu_3(trz)_3(\mu_3\text{-}OH)]Cl_2.6H_2O$ at Low Temperature. Biodiversity Online J. 5(4). BOJ. 000618. 2025.
DOI: 10.31031/BOJ.2025.05.000618

Abstract

Bojarite Mineral $[Cu_3(trz)_3(\mu_3\text{-}OH)]Cl_2.6H_2O$ was prepared at two temperatures (120 and 150 °C) by hydrothermal route for the first time. The sample was characterized by X-ray Diffraction (XRD), thermal analysis (TG/DTG) and Raman spectroscopy. The XRD analysis shows peaks attributed to Bojarite, crystallizing in a cubic structure. The Raman spectrum displays the characteristic bands of the Bojarite. The TG/DTG profile shows that the product contains water and organic matter, consistent with the nominal composition. A direct optical transition of gap Eg (=2.26eV), determined from the diffuse reflectance correspond to the transition $O^{2-}:2p\rightarrow Cu^{2+}:t_{2g}$. The photoelectrochemical has also been undertaken. Voltammetry in Na_2SO_4 solution (0.1M) exhibits low exchange current density (~2mAcm^{-2}) and good electrochemical stability. The variation of interfacial capacitance versus potential is typical of n-type behavior with an electron density of 3.12×1016cm^{-3} and a flat band potential (E_{fb}) of 0.17 VSCE. The Electrochemical Impedance Spectroscopy (EIS) shows only the bulk contribution in the dark (22kΩcm^{-2}), which decreases to 12.7kΩcm^{-2} under visible irradiation supporting the semi conductivity. The positioning of the conduction and valence bands allows us to conclude that this material can be used in electrolysis.

Keywords: Bojarite; Hydrothermal synthesis; Thermal analysis; Photoelectrochemistry; Electrolysis

Introduction

Hybrid porous solids designate a class of material whose crystal lattice is composed of organic and inorganic parts. The development of these materials, resulting from the association of coordination chemistry with solid-state chemistry combined with the richness of organic chemistry, has evolved very slowly. The term coordination polymers were proposed early in 1964 to designate these hybrid materials whose porosity was demonstrated in the 1970 [1]. It was only from 1989 that interest in these compounds was expanded, notably with the work of Hoskins et al. Robson who demonstrate the possibility of generating three-dimensional structures by coordination from the association of organic and inorganic entities since there. The chemical and physical property of porous coordination polymers has experienced a considerable growth over the last decades [2]. These metal-organic systems, often referred to by the acronym MOF's (Metal Organic Framework), have made it possible to access materials to combining remarkable porosities and one, or many, additional physical properties. The vast majority of MOF's described in the literature were obtained from divalent 3d metals (Cu^{2+}, Zn^{2+},Fe^{2+},Mn^{2+},Co^{2+} ,Ni^{2+}) [3], a few from trivalent transition metals (Sc^{3+}, Cr^{3+}, Fe^{3+}, La^{3+}) [4], and very little with trivalent elements of the p block of the periodic Table (Al^{3+}, Ga^{3+}, In^{3+}) [5].The first metal-organic compound $K_2Zn_3[Fe(CN)_6]_2.xH_2O$ was reported in the 1970 [6] and its three-dimensional skeleton is of the zeolitic type. The synthesis of the first structure bearing the MOF terminology, named MOF-5, was synthesized in 1999 [7].

Nowadays, the Metal-Organic Frameworks (MOFs) are of great interest enthusiasm both academically and industrially which is given its vast range of applications in fields as varied as catalysis [8], gas storage [9], separation [10], sensors [11], adsorption [12], antimicrobial properties [13] and photocatalysis [14]. The node and spacer technique are among the most used synthetic strategies for designing open-framework hybrid materials. It uses metal ions attachment sites for dipodal or multipodal linkers. Moreover, stable designs have been achieved by using metal clusters as nodes as opposed to individual metal ions. Synergizing the properties of organic/inorganic components is difficult for such hybrid compounds. An increasing number of intriguing compounds have been produced by interacting metal oxides with organic molecules or metal-organic coordination fragments. One such ligand is the polyaza heterocycle 1, 2, 4-triazole (HTAZ), which possesses a super exchange capacity and can create bridge metal ions to obtain polynuclear complexes. When searching for methods for new organic-inorganic hybrid materials from molecular building blocks, we examined the role of ligand "trz in Cu II–trz" coordination cations, used to from new complexes [15] and coordination compounds including this class of ligands coordinated to 3d metal ions like Cu [16], Co [17] and Fe [18]. The aim of the present work is to report the effect of the temperature on the preparation of the Bojarite and physical and photo-electrochemical characterization are reported and discussed for the first time.

Experimental

Syntheses

All chemicals' reagents were commercially purchased and used without any other purification. In a typical synthesis, 0.51g of $CuCl_2$, $2H_2O$, was first dissolved in 22.5ml of H_2O, followed by 0.27g of 1, 2, 4 triazole (HTAZ) and finally, 0.98g of KOH was added to the above solution. The temperature was fixed at 120 and 150 °C.

Characterization

Powder diffractograms were obtained with a Panalytical X'Pert Pro diffractometer equipped with an infiltered monochromatic Cu (Kα) radiation (λ=0.154nm). The measurements were carried out at room temperature, using the Bragg-Brentano geometry, a step of 0.02° was used in the range (5–60°) with a step-by-step scanning mode. The counting time was set at 2 seconds per step, allowing precise and reliable data for analysis. Raman spectra were recorded with the Renishaw in Via Raman microscope, in the range (200-1400cm^{-1}), using an excitation wavelength of 758nm. TGA/DSC Instruments SDT Q600 thermo-balance was used to conduct the thermal analysis from 25 to 800 °C under N_2 atmosphere. UV-Vis spectrum was recorded between 190 and 900nm thanks to UV-Vis spectrophotometer (Model Jasco V-650) with $BaSO_4$ as standard. The cyclic voltammetry was performed in a three-electrode cell filled with Na_2SO_4 (0.1M) and containing the working electrode, the Saturated Calomel Electrode (SCE) and Pt counter electrode. The cell was connected to a computer-controlled potentiostat (galvanostat Software Model NOVA 8.1). All measurements were performed in the Standard Temperature And Pressure (STP). The Mott Schottky curve was traced at a frequency (10kHz), to eliminate parasitic effects. The Electrochemical Impedance Spectroscopy has also been undertaken, the measurement was carried out between 10^{-2} and 105Hz in the dark and under visible light.

Results and Discussion

Characterization

We adjusted the temperature at 120 then at 150 °C allowed to obtain the products (1) and (2) respectively. An in-depth analysis of these compounds was carried out to determine the effect of this thermal variation.

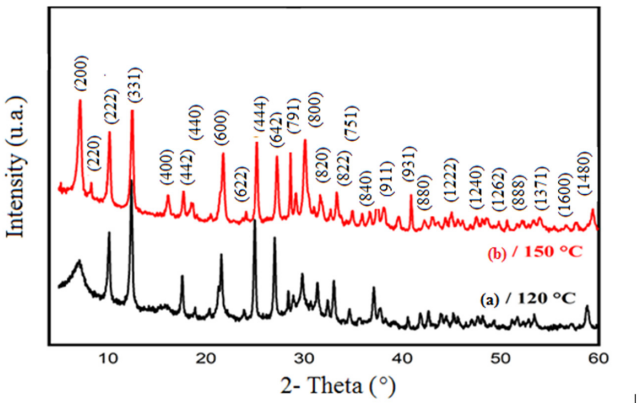

Figure 1: Effect of the temperature on XRD patterns of the Bojarite.

The diffractograms presented in (Figures 1a & 1b) show that all peaks are indexed in the cubic structure of the copper triazolate mineral (Bojarite) the mineral was discovered in the Pabellón de Pico Mountain, Chile. This structure agrees with the ideal formula of the Bojarite $[Cu_3(trz)_3(\mu_3\text{-}OH)]Cl_2.6H_2O$ (CCDC-796529), reported previously with the lattice parameter: a=24.8047(5) and the space group (SG: Fd3c) [19]. The Raman spectrum of the sample is presented in (Figure 2), its analysis made it possible to assign the different bands observed, thus revealing valuable information on the molecular vibrations and chemical interactions present in the Bojarite. The peaks 968, 1311 and 931cm^{-1} are attributed to the elongation and deformation vibration in the plane of 1, 2, 4 triazole. While those at 369 and at 260cm^{-1} are assigned to the elongation vibrations of Cu-O and Cu-N groups. The peak centered at 1000cm^{-1} is due to degenerate antisymmetric stretching vibrations ($A_{1g}+E_g$) of the phosphate ligands [20]. The optical gap, important parameters in photovoltaic and photocatalysis, enales to quantify the solar fraction converted in useful energies. The thermogram of Bojarite (Figure 3) shows a progressive weight loss of ~10% up to 150 °C, attributed to the dehydration of the water belonging to the crystal structure. This weight loss is accompanied by an endothermic peak on the DSC curve. Then, a two-step loss is observed in the temperature between range (300-700 °C), accounting for a total decrease of 39% of the initial mass, due to the complete decomposition of the organic part Htrz. The absorbance spectrum of the Bojarite (Figure 4a) shows two distinct peaks (215 and 257nm) corresponding to the metal-oxygen charge transfer, as well as a broad band observed at 650nm attributed to internal d-d transitions of Cu^{2+} in an octahedral coordination. The Kubelka-

Munk function was used to determine the transitions from the diffuse reflectance:

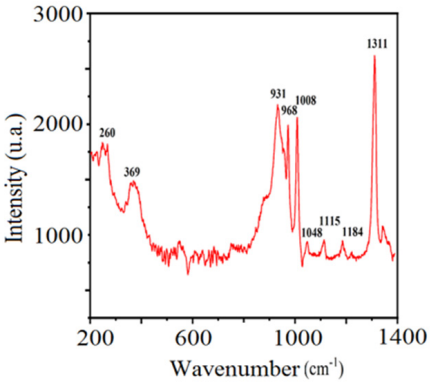

Figure 2: Raman spectrum of the Bojarite prepared at 150 °C.

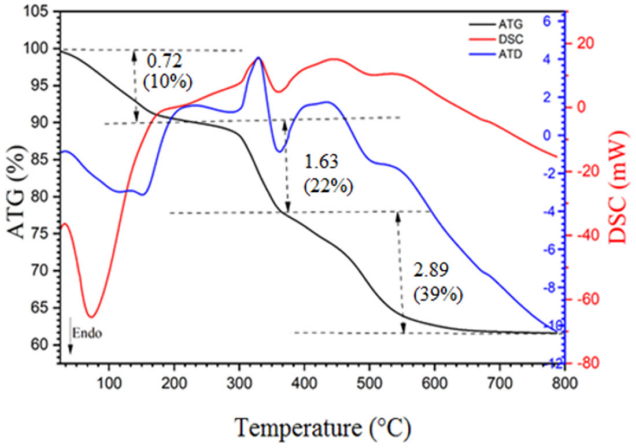

Figure 3: Combined TG/DTG/DSC profiles of the Bojarite synthetized by hydrothermal route.

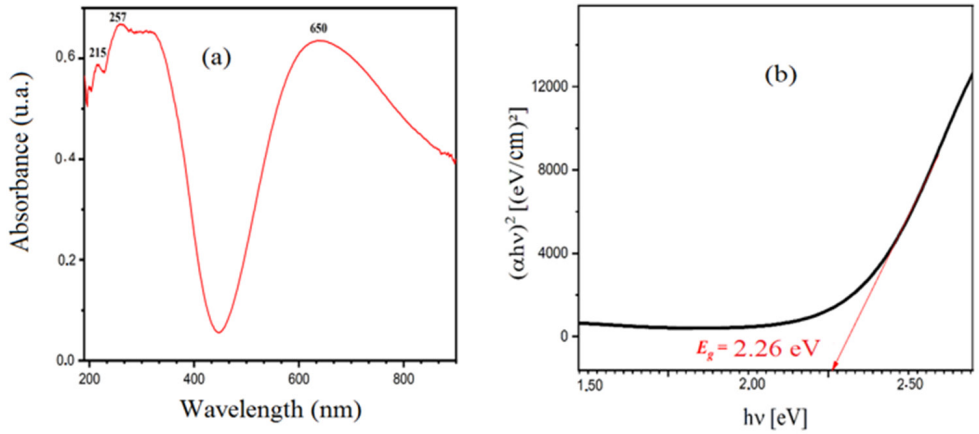

Figure 4: Absorbance spectrum (a) and direct optical transition of the Bojarite (b).

$$F(R)=\frac{(1-R)^2}{2R} \quad (1)$$

The gap E_g is reliably evaluated from the well-known relation:

$$(\alpha_\lambda h\nu)^{1/k}=Constant\times(h\nu-E_g) \quad (2)$$

where the integer k is equal to 2 or 1/2 respectively for indirect or direct transition. The line $(\alpha_\lambda h\nu)^2$ as a function of hν shows a direct transition at 2.26eV (Figure 4b). Such value comes from the electron transfer from oxygen lone pair O^{2-}: 2p to the low spin Cu^{2+}: t_{2g} octahedrally bonded and makes it possible to exploit ~40% of the sun spectrum. The direct gap is the energy difference between the top of the Valence Band (VB) and the bottom of the Conduction Band (CB) and without phonon assistance. The following relations give (the energy / potential) of CB and VB:

$$P_{CB}=4.75+|e|\times E_{fb}+E_a \quad (3)$$

$$P_{VB}=P_{CB}-E_g \quad (4)$$

Bojarite-CB (4.72eV /-0.03 V) indicates that the conduction band is typical of materials with valence band (CB) deriving mostly from O^{2-}: 2p orbital while VB is made up of Cu^{2+}: t_{2g} orbital the latter is positioned at (6.98eV / 2.23V).

Photo electrochemical characterization

The photo electrochemical study of $Cu_3(trz)_3(\mu_3\text{-}OH)]Cl_2.6H_2O$ is reported for the first time. The J(E) graph (Figure 5) is more or less symmetric, with a current density in the dark (J_d) smaller than 0.1mAcm^{-2}. The oxygen reduction occurs at ~-0.5V in agreement with the literature ($O_2+2H_2O+2e^-\rightarrow H_2O_2+2OH^-$) [21]. The increased current (J_d) above 1.2V corresponds to oxygen production ($H_2O+2h^+\rightarrow 0.5O_2+2H^+$) with a high over voltage (0.6V). On the other hand, the current decreases below ~-1V is due to H_2 release as evidenced by gas bubbles on the electrode. The Bojarite/solution junction is assimilated to a planar capacitor with plates having a surface area (S), separated by a length (d) and permittivity ε (C=εεo/k), k being the form factor (=d/S) and ε_o the permittivity of vacuum (8.82x10^{-14}Fcm^{-1}). The capacitance of the depletion width (CdW) is counter balanced by the double layer (C_{dl}):

$$C^{-1}=C_{dw}^{-1}+{}_{dl}^{-1} \quad (5)$$

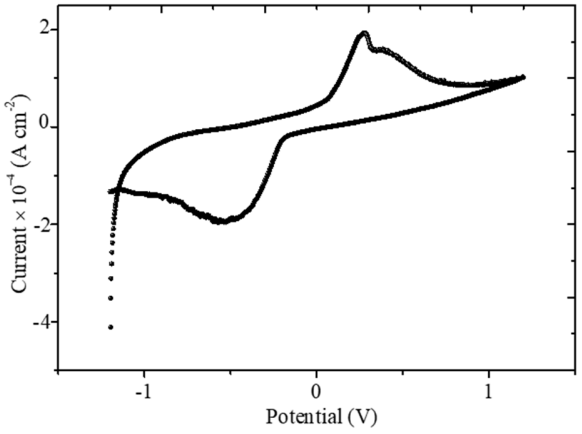

Figure 5: The J(E) characteristic of the Bojarite plotted in Na_2SO_4 solution.

However, the low carrier density of the Bojarite (see below) makes the capacitance of the double layer C_{dl} negligible and the flat band potential (Efb=0.17V) is accurately determined from the relationship:

$$C_{dw}^{-2} = \{2 / \varepsilon_0 e \varepsilon N_D\} \{E_{fb} - E\} \quad (6)$$

The positive slope of the line (Figure 6) is characteristic of n-type semiconductor with electrons as dominant carriers. By using the Electrochemical Impedance Spectroscopy (EIS), it is possible to distinguish the contributions of the bulk, grains boundaries and diffusion at the SC/solution interface. The curve Z_{im} against Z_{real} (Figure 7) does not show an inclined line at low frequencies eliminating the diffusion process. The diameter of the semicircle decreases from 22 in the dark to 13Ωcm^2 under visible illumination thus corroborating the semiconducting-like behavior of the Bojarite. The offset from the origin (1.8kΩcm^2) correspond to the electrolytic solution due to the mobility of Na^+ (52m^{2}V^{-1}s^{-1}) and ½ SO_4^{2-} (80m^{2}V^{-1}s^{-1}). The electrochemical properties seem suitable for water treatment and oxygen production by photocatalysis. Preliminary results are satisfactory and details will be communicated later.

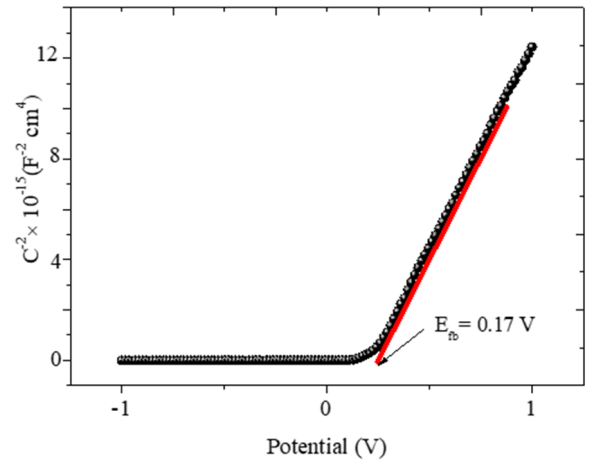

Figure 6: The variation of the capacitance (C^{-2}) as a function of the potential (E) of the Bojarite in Na_2SO_4 solution.

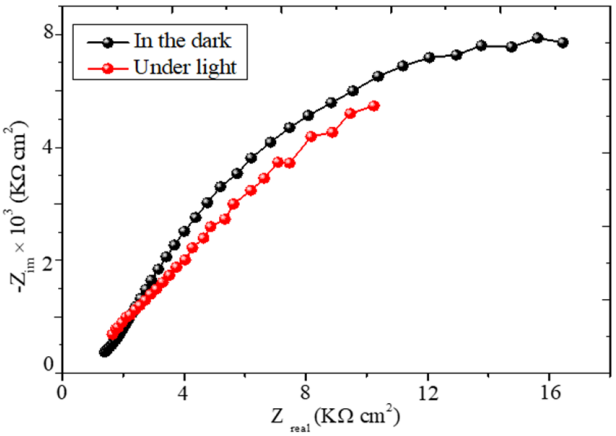

Figure 7: The EIS representation in the dark and under illumination of the Bojarite in Na_2SO_4 solution.

Conclusion

This work reports the synthesis and characterization of $[Cu_3(trz)_3(\mu_3\text{-}OH)]Cl_2.6H_2O]$ obtained hydrothermally by varying the temperature. The thermal effect allowed identifying the formation of the compound at 120 and 150 °C. The physical and photoelectrochemical characterization were investigated. The Raman spectrum showed the characteristic bands of the Bojarite. The combined TG/DTG/DSC curves confirmed the presence of water and triazole structurant. The diffuse reflectance displayed a direct optical transition with a gap value Eg of 2.26eV, due to the charge transfer O^{2-}: 2p→Cu^{2+}: t_{2g}. The J (E) profiles exhibit an electrochemical stability with a sluggish redox process due to $Cu^{2+/+}$ couple. The variation of interfacial capacitance versus potential is typical of n-type behavior. The EIS analysis corroborated the semiconductor behavior of the Bojarite with predominant bulk contribution. The as-prepared material can used in photolysis of water

Authors Contributions

RB contributed to the methodology and writing of the draft manuscript, WD software, AL software, AMD Photoelectrochemical Analysis, MT contributed to the final drafting of the manuscript.

References

1. Stock N, Biswas S (2012) Synthesis of Metal-Organic Frameworks (MOFs): Routes to various MOF topologies, morphologies, and composites. Chem Rev 112: 933-969.
2. Jet-Sing LM, Otake K, Kitagawa S (2020) Transport properties in porous coordination polymers. Coordination Chemistry Reviews 421: 213447.
3. Rehman A, Khan A, Pervaiz E (2024) The role of nickel cobalt sulphide MOFs hybrids in electrochemical hydrogen generation: A critical review. Materials Chemistry and Physics 315: 129027.
4. He Q, Zhao H, Teng Z, Guo Y, Ji X, et al. (2024) Tuning microscopic structure of La-MOFs via ligand engineering effect towards enhancing phosphate adsorption. J Environmental Management 353: 120149.
5. Sun H, Tang X, Zhang J, Li S, Liu L (2021) MOF-derived bow-like Ga-doped CO_3O_4 hierarchical architectures for enhanced triethylamine sensing performance. Sensors and Actuators B: Chemical 346: 130546.

6. Gravereau P, Garnier E, Hardy A (1979) Les hexacyanoferrates zéolithiques: Structure cristalline de $K_2Zn_3[Fe(CN)_6]_2.xH_2O$. Acta Cryst B35: 2843-2848.
7. Li H, Eddaoudi M, Keeffe OM, Yaghi OM (1999) Design and synthesis of an exceptionally stable and highly porous metal-organic framework. Nature 402: 276-279.
8. Zhang Y, Yu X, Hou Y, Liu C, Xie G, et al. (2024) Current research status of MOF materials for catalysis applications. Molecular Catalysis 555: 113851.
9. Jia T, Gu Y, Li F (2022) Progress and potential of Metal-Organic Frameworks (MOFs) for gas storage and separation: A review. J Environmental Chemical Engineering 10: 108300.
10. Amooghin AE, Sanaeepur H, Ghomi M, Luque R, Garcia H, et al. (2024) Flexible-robust MOFs/HOFs for challenging gas separations. Coordination Chemistry Reviews 505: 215660.
11. Mohan B, Priyanka, Singh G, Chauhan A, Pombeiro AJL, et al. (2023) Metal-Organic Frameworks (MOFs) based luminescent and electrochemical sensors for food contaminant detection. Journal of Hazardous Materials 453 :131324.
12. Lei Y, Xie J, Wang A (2024) Advances in adsorption of Pb(II) by MOFs-based nanocomposites in water. Progress in Natural Science: Materials International 34(1): 122-146.
13. Li Y, Han Y, Li H, Niu X, Zhang D, et al. (2024) Modification of a rod-shaped Bi-MOF with MoS_2 nanosheets to form a p-n heterojunction for enhanced antimicrobial activity. Applied Surface Science 654: 159434.
14. Bagtache R, Rekhila G, Abdmeziem K, Trari M (2014) Characterization of a copper phosphate triazole metal organic framework material $(Cu_3PO_4(C_2N_3H_2)_2OH)$ and oxygen evolution studies. Materials Science in Semiconductor Processing 23: 144-150.
15. Bagtache R, Meziani D, Abdmeziem K, Trari M (2021) Synthesis, Physical And photo-electro chemical characterizations of a new hybrid host-guest complex $[Cu_{12}(C_2N_3H_2)_8Cl][(PW_{12}O_{40})]$. Journal of Molecular Structure 1227: 129718.
16. Bagtache R, Malaman B, Abdmeziem K (2010) Synthesis and structure of Cu_3PO_4 [1, 2, 4-triazole]$_2$OH with a hybrid layered structure: A new organically templated copper (II) hydroxyphosphate. Solid State Sciences 12: 1178-1182.
17. Hassen S, Arfaoui Y, Steenhaut T, Filinchuk Y, Klein A, et al. (2023) A cationic Co(II) coordination polymer $1_\infty[Co(\mu\text{-}L)(\mu\text{-}Cl)(H_2O)_2]^+$ with the 4-amino-4H-1,2,4-triazole ligand: Structure, thermal behavior, and antimicrobial activity. Inorganica Chimica Acta 557: 121664.
18. Kharadi GJ (2013) Antioxidant, tautomerism and antibacterial studies of Fe(III)-1,2,4-triazole based complexes. Spectrochimica Acta Part A: Molecular and Biomolecular Spectroscopy 110: 311-316.
19. Yamada T, Maruta G, Takeda S (2011) Reversible solid-state structural conversion between a three-dimensional network and a one-dimensional chain of cu(ii) triazole coordination polymers in acidic/basic-suspensions or vapors. Chem Commun 47: 653-655.
20. Qi J, Lin YP, Chen D, Zhou T, Zhang W, et al. (2020) Autologous cobalt phosphates with modulated coordination sites for electrocatalytic water oxidation. Angew Chem Int Ed 59: 8917-8921.
21. Robert CW (1975) Handbook of chemistry and physics. (56th edn), pp. 1-2351.